Original article

Institution of MECHANICAL ENGINEERS

Journal of PROCESS MECHANICAL ENGINEERING

Depriving friction stir weld defects in dissimilar aluminum lap joints

Proc IMechE Part E:
J Process Mechanical Engineering
1–12

DOI: 10.1177/09544089241239817
journals.sagepub.com/home/pie
Sage

S Suresh[1], Elango Natarajan[2,3], Dhanesh G Mohan[4,5], Chun Kit Ang[2] and S Sudhagar[6]

Abstract

The contemporary automotive industry increasingly incorporates composite materials and innovative joining techniques to meet customer demands for lightweight, high-strength alloys. This research explores the feasibility of using friction stir welding (FSW) methods to fabricate dissimilar aluminum nanocomposite lap joints, integrating Al_2O_3 nanoparticles into the weld nugget. Lap joints were prepared with varying tool rotation speeds (1000–1600 rpm) and the mechanical and metallurgical behaviors of AA6061–AA7075-T6/Al_2O_3 lap joints were examined. The inclusion of filler material in the weld joint resulted in an 18% increase in shear strength compared to joints without filler. Dynamic crystallization impeded grain boundaries and reduced grain size in the weld stir zone (SZ), with the most enhanced mechanical characteristics observed at a tool rotation speed of 1400 rpm. The shear strength at 1400 rpm was 5780 N, representing a 17% increase compared to joints prepared at 1000 rpm. Field emission scanning electron microscopic examination revealed evenly dispersed Al_2O_3 nanoparticles within the weld zone, supporting the lap shear test results. Notably, joints created at lower (1000 rpm) and higher tool rotational speeds (1600 rpm) exhibited brittle fracture behavior. The addition of Al_2O_3 significantly improved lap joint tensile strength due to its uniform dispersion in the SZ. Increasing the FSW tool rotational speed from 1000 to 1400 rpm facilitated nanoparticle dispersion, further enhancing lap joint strength.

Keywords

Lap joint, FSW, dissimilar weld, Al_2O_3, nanoparticles

Date received: 4 October 2023; accepted: 29 January 2024

Introduction

The automotive industry is increasingly adopting lightweight, high-strength alloys such as aluminum, magnesium, titanium and fiber-reinforced plastics to enhance fuel efficiency, reduce CO_2 emissions and improve design aesthetics.[1,2] Aluminium is becoming increasingly important in contemporary automobile manufacturing, particularly for applications related to the vehicle's structural components.[3,4] This is primarily attributed to its low density, high specific strength and outstanding corrosion resistance, making it a preferred choice in this regard.[5–7] The potential of 7XXX aluminum alloys has been explored for various sectors like renewable energy industries and marine industries.[8] Fuel tanks are one of the applications where Al alloys or metal matrix composites have been employed. However, fusion-based welding techniques used for joining aluminum alloy parts often result in weak welds due to excessive heat generation.[9–11] Joining thin aluminum alloy sheets necessitates careful attention to prevent issues such as sheet wrapping, which can be addressed by minimizing heat input and utilizing a clamping device.[12,13]

Addressing the limitations of fusion welding, especially in joining dissimilar aluminum alloys with varying chemical compositions, mechanical properties and thermal characteristics, has become a critical focus of research.[14,15] Formation of brittle intermetallic compounds and undesirable microstructural changes that lead to low weld strength are encountered in conventional fusion welding.[16,17] Alternative joining techniques that

[1]Department of Mechanical Engineering, Erode Sengunthar Engineering College, Erode, India
[2]Faculty of Engineering, Technology and Built Environment, UCSI University, Kuala Lumpur, Malaysia
[3]Department of Mechanical Engineering, PSG Institute of Technology and Applied Research, Coimbatore, India
[4]School of Engineering, Faculty of Technology, University of Sunderland, Sunderland, UK
[5]Centre of Research Impact and Outcome, Chitkara University Institute of Engineering and Technology, Chitkara University, Punjab, India
[6]Department of Mechanical Engineering, Kalaignarkarunanidhi Institute of Technology, Coimbatore, India

Corresponding author:
Elango Natarajan, Faculty of Engineering, Technology and Built Environment, UCSI University, Kuala Lumpur, Malaysia; Department of Mechanical Engineering, PSG Institute of Technology and Applied Research, Coimbatore, India.
Email: cad.elango.n@gmail.com

can overcome these limitations and provide robust, reliable and high-quality joints are of great interest and research.[18–20] As a result, the demand for friction stir welding (FSW) in the manufacturing industry is significant due to its numerous advantages over conventional joining methods.[21–23] The quality of an FSW joint is subjected to multiple influencing welding parameters like tool profile, tool rotational speed, feed and depth of shoulder penetration.[24–26] Among these parameters, tool rotational speed is a critical parameter in ensuring the formation of high-quality joints.[27–31] The FSW technique has gained widespread attention among researchers worldwide, particularly in the context of welding dissimilar metals. Given the varying microstructures and mechanical properties observed in FSW joints of thin sheets due to heat dissipation and insufficient material flow,[32–35] it is imperative to explore alternative methods or strategies for joining lightweight alloys. In the context of FSW-lap joints, the positioning of the base material (BM) plays a crucial role in influencing material flow dynamics and contributes to the occurrence of a common welding defect known as the “hook.” This defect manifests in various sizes and is a consequence of the material movement, which occurs in an upward direction from the bottom sheet to the top sheet. As anticipated, the size of the hook defect is not only influenced by the rotational speed and welding speed but is also significantly impacted by the initial placement of the BM.[36,37] Over the past few decades, there has been an increasing fascination with the integration of ceramic particles into the adjacent face during FSW and friction stir processing (FSP).[38–44] The addition of ceramics may result in increased or decreased strength based on the particles agglomeration during the process of FSW. For example, in a study by Babu et al.,[45] it was experiential that incorporating agglomerated fillers led to a notable decrease in the mechanical strength of joints in nickel-based metal matrix composites. West et al.[46] observed that even minor changes in the size of reinforcement particles during FSW could have a notable impact on the hardness of the resulting composite joint. Consequently, it becomes apparent that introducing finely dispersed ceramic nanoparticles into the weld area holds promise for improving weld characteristics. However, the challenge of preventing the agglomeration of particles remains an ongoing issue that requires further investigation.

In the past few decades, notable research has been conducted on joining dissimilar aluminum alloys in a lap configuration to enhance the mechanical behavior of lap joints. Abbass et al.[47] introduced an innovative method known as friction stir diffusion welding. This technique was employed for the creation of lap joints, utilizing AA110 and AA6061-T6 alloys as the materials of choice. They could achieve the joint efficiency of 93% at rotation speed = 1250 rpm and traverse speed = 75 mm/min. In the context of dissimilar welding of 5× and 6× aluminum alloys without nanoparticle reinforcement, previous research as documented in references[48–50] has signified that the heat input is influenced by the welding tool’s rotational and traverse speed. In another study, using FSW, Jasiūnienė et al.[51] investigated SiC reinforcement overAA6082-T6 and AA5083-H111 dissimilar joints. After conducting high-frequency ultrasonic tests, they reported that welding direction significantly influences weld quality, and even small flaws can substantially impact joint performance.

Kumar et al.[52] recently introduced a zinc interlayer during the preparation of FSW butt joints on dissimilar AA6061/AZ61 alloys and showed enhanced tensile properties and corrosion resistance due to incorporation of the zinc interlayer. In another study, Saleh et al.[53] fabricated dissimilar FSW joints of AA1050 and S45C with zinc (Zn) interlayers and compared them with a joint without any interlayer. The presence of a zinc interlayer and the formation of zinc-rich particles along the grain boundaries of A1050 enhanced the weld strength by facilitating discontinuous dynamic recrystallization.

Carbon nanotubes (CNT) reinforced FSW aluminum alloys were reported by Rabiezadeh[54] in which authors revealed that hardness, wear resistance and joint efficiency (>100%) were obtained under some specific conditions and the ductile fracture was the primary failure mechanism. The friction coefficient decreased by about 30% in two-pass welded samples compared to the base metal (BM). These findings contribute valuable insights into the potential benefits and limitations of CNT in dissimilar aluminium alloy welding processes. According to the existing body of literature, it becomes evident that introducing nanoparticles into the welding zone exerts a substantial influence on the metallurgical attributes while concurrently diminishing the occurrence of intermetallic compound formation at the stir zone (SZ). It also decreases the grain size in the heat-affected zone FSWed joints.[55,56]

However, using SiC or CNT as a reinforcement filler in certain applications is not advisable, as both materials have higher electrical conductivity, high cost and complexity in production. Alternatively, Al_2O_3 is the better choice of ceramic materials, which have good strength, high thermal conductivity, high corrosive resistance and high abrasive characteristics. On top of it, it is abundantly available eco-friendly material. Incorporating nano Al_2O_3 can further enhance the mechanical and functional characteristics of the weld despite the challenge of the filler distribution over the nugget zone persists. There is a shortage of research on dissimilar lap joints, and thus, the mechanical and corrosive properties of reinforced FSW lap joints must be investigated and published. As weld quality primarily depends on influencing process parameters, particularly the tool rotation speed, this study aims to assess the feasibility of FSW for fabricating AA6061-T6/AA7075-T6 dissimilar aluminum nano-composites lap joints and evaluating the optimal rotational speed of the tool that could yield the highest weld quality. At this end, the paper is organized with results and discussion in the third section, while the second section explains the method of research.

Experimental design

Materials and tool

Dissimilar 6061-T6 and 7075-T6 aluminum alloy plates measuring 100 × 100 × 2 mm were fabricated using Electrical Discharge Machining (EDM). The properties of these alloys are presented in Supplemental Table S1. 6061-T6 alloy has Si that resulted in improved strength and heat treatability. In contrast,7075-T6 alloy has significant Zn towards increased strength and hardness. While 6061-T6 and 7075-T6 aluminum alloys are widely used in various applications, their differing compositions result in distinct mechanical properties that make a combination of these alloys more suitable for specific structural needs demanding high strength and lightweight.

Al_2O_3 of particles in the range of 40–50 nm with a purity of 99% was used to reinforce the nugget zone of the weld. Figure 1(a) shows transmission scanning microscopic image and energy dispersive spectrometer results. AISI H13 steel tool was customized and used in FSW experiments, wherein the length of the tool pin = 2.85 mm and the diameter of the cylindrical shoulder = 5 mm. The detailed dimensions of the FSSW tool are illustrated in Figure 1(b)). The fabricated tool underwent a heat treatment process to achieve a hardness of 58 Rockwell C, enhancing its durability and wear resistance when utilized in the FSW operation.

Weld samples preparation

Customized CNC vertical machining centre (make-ACE micrometric) was used for preparing lap-FSW (LFSW) samples as illustrated in Figure 2. To embed the Al_2O_3 nanoparticles, a square groove was created on the overlapped top sheet along the welding direction and 5.5 vol% of Al_2O_3 nanoparticles were added into the groove. This volume fraction was determined based on the slot and tool dimension.[57] To investigate the impact of rotational speed, various rotational tool speeds were considered: 1000, 1200, 1400 and 1600 rpm. Prior research and studies were conducted to establish these parameter ranges respective to the selected materials.[57]

Throughout experimentation, tool travel speed, shoulder plunge depth and tilt angle were maintained as 15 mm/min, 0.2 mm and 0, respectively. A total of 12 samples were prepared (three samples in each tool speed), as some samples shown in Figure 3.

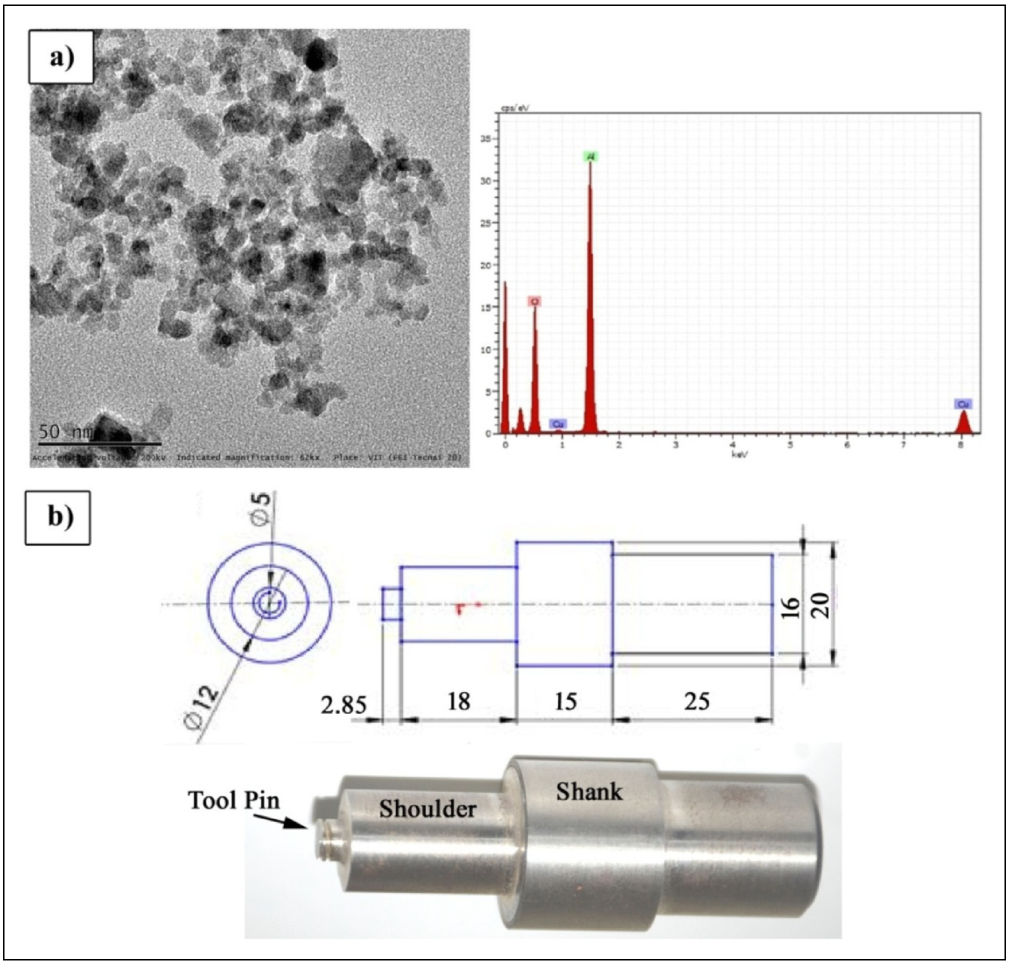

Figure 1. (a) TEM image and EDS of the Al_2O_3 nanoparticles and (b) dimensions of FSW tool.

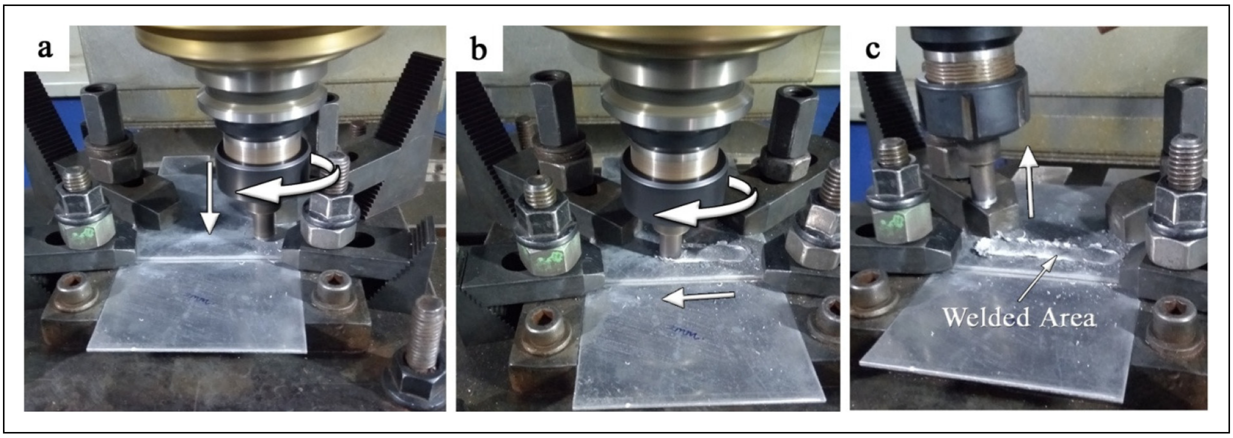

Figure 2. Process sequence of lap-FSW process.

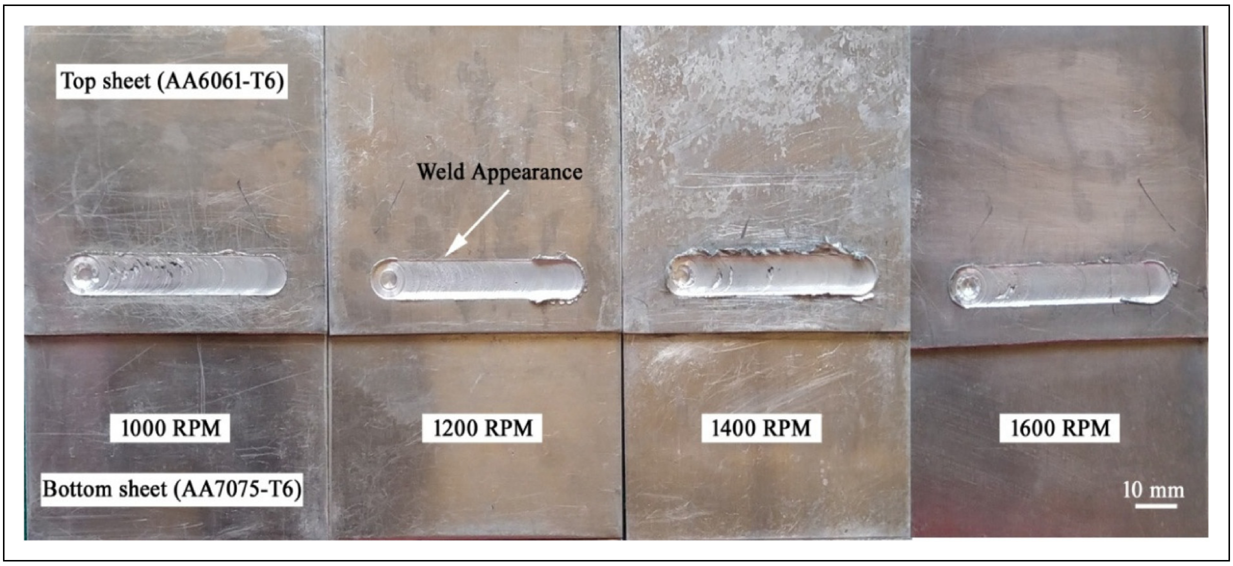

Figure 3. Fabricated FSW lap joint samples.

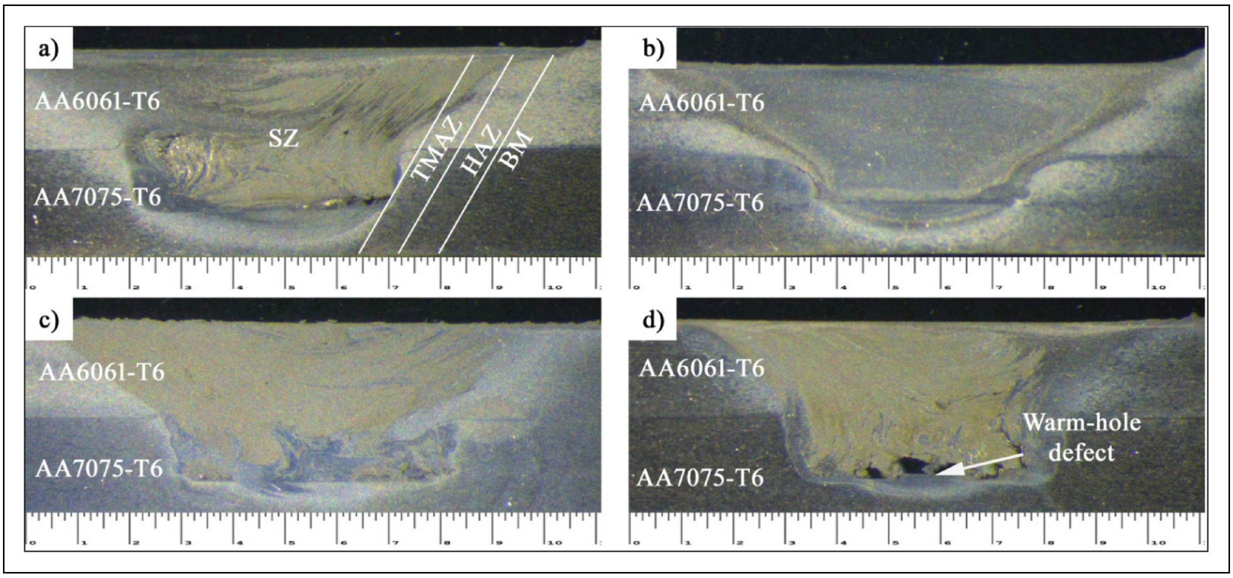

Figure 4. Cross-sectional macrostructure of welded samples at different tool rotational speeds (a) 1000, (b) 1200, (c) 1400 and (d) 1600 rpm.

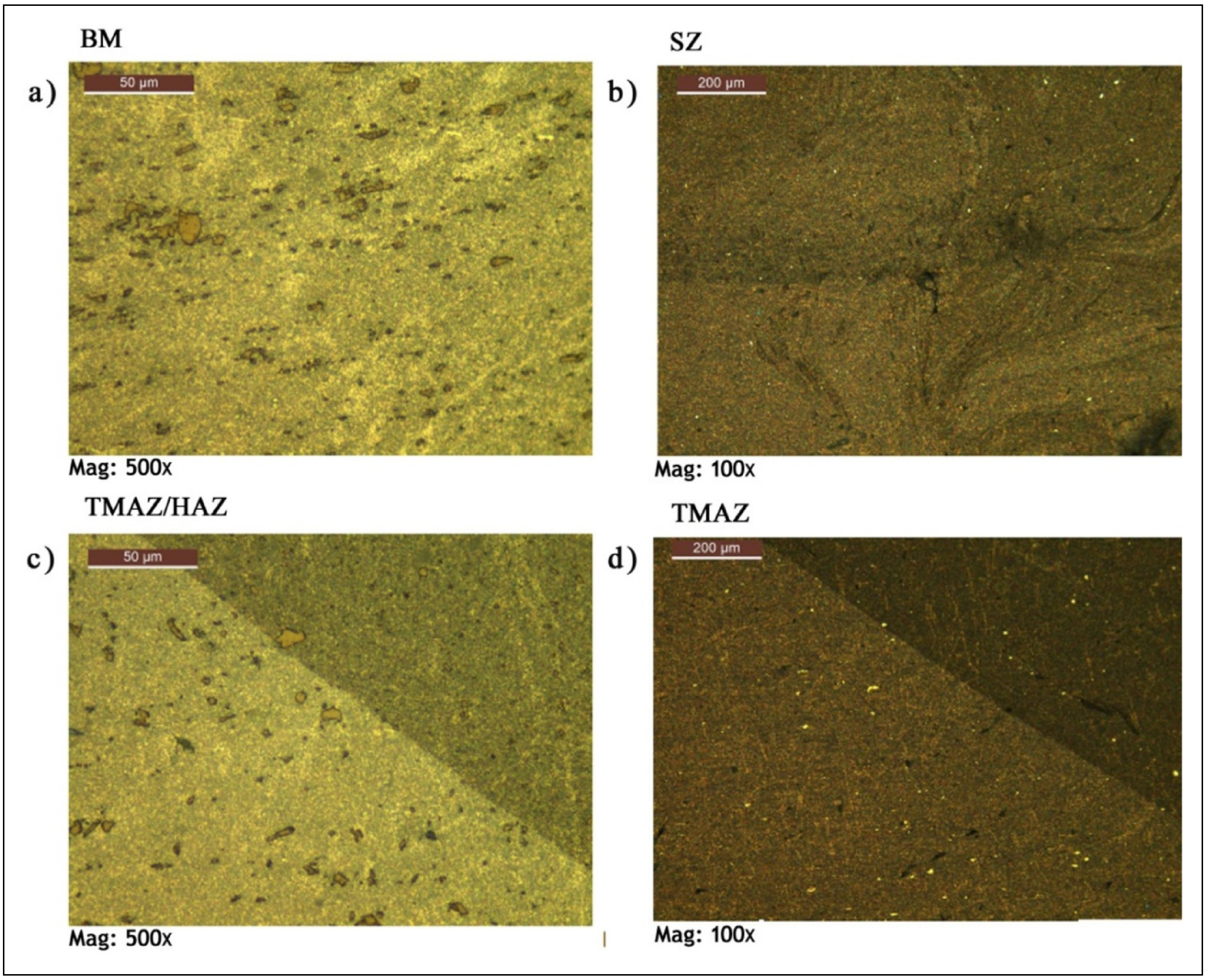

Figure 5. Optical micrograph across the cross-section of the 1400 rpm joints (a) BM, (b) SZ, (c) TMAZ/HAZ and (d) TMAZ.

Testing and characterization

After employing FSW welding, specimens measuring 100 × 40 mm were meticulously sectioned utilizing a wire-EDM machine. Subsequently, the lap shear strength of the resultant overlap joints was assessed in accordance with ASTM D1002 standards using a computerized universal testing machine (TE-JINAN-WDW100). The lap shear experiment was performed at room temperature with a crosshead speed of 1 mm/min, and the average result from three separate specimens under each welding condition was calculated.

Macro and microstructure analyses of the joint cross-sections were conducted to understand the structural characteristics of the welds. A stereo zoom microscope (Radical RSM-9, Radical Scientific, India) was utilized for an initial macroscopic examination, followed by detailed observations using an optical microscope (Invertoplan TR, Gippon-Japan). Standard metallographic assessment of samples, etched with Keller's regent (5 ml HNO_3, 3 ml HCl, 2 ml HF and 190 ml H_2O), provided insights into the microstructural features of the welds. Nanoparticle dispersion within the weld zone was assessed using a field emission scanning electron microscope (ZEISS SIGMA, Germany).

Results and discussion

Macro and microstructure

Macrostructure of friction stir welded AA6061-T6/AA7075-T6 joints under different tool rotational speeds (1000 rpm to 1600 rpm) are presented in Figure 4. SZ, thermo-mechanical affected zone (TMAZ) and heat affected zone (HAZ) as indicated by the lines in Figure 5 are considered for the analysis as high heat generation and intense plastic deformation are characteristics of FSW.

The stir zone width in the macrostructures of all welded joints is depicted in Figure 4. Evidently, as the rotation speed (and consequently, the heat input) increases, the stir zone width also increases, resulting in a flatter and more homogeneous nugget. Additionally, it is worth mentioning that the sizes of TMAZ and HAZ exhibit variations. In summary, it can be inferred that the tool's rotational speed exerts a substantial influence on both heat input and material flow within the welded zone, thereby leading to distinct macrostructural characteristics in the welded joints.

It is worth noticing the wormhole defect at the end of SZ of the specimen made at 1600 rpm (as shown in

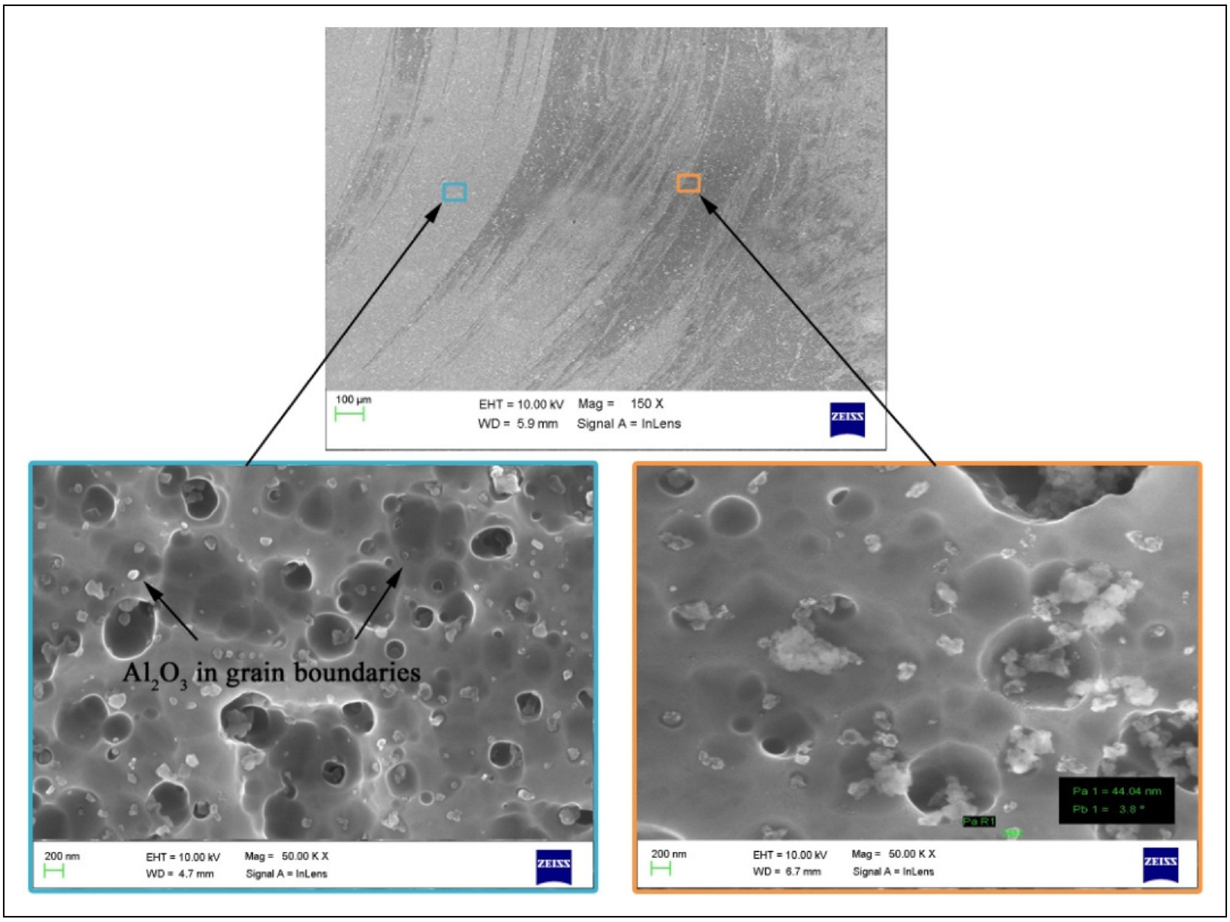

Figure 6. FESEM image of SZ at 1400 rpm tool speed.

Figure 4(d)). It is because of higher heat generation at SZ that significantly affects the material flow. It is augmented that 1400 rpm is the optimal rotational speed to be used in FSW of these dissimilar Al alloys.

Distinct grain sizes were observed in FSWed samples, and hence, high magnification images of the different zones of the sample made at 1400 rpm are shown in Figure 5 to provide a better understanding of the microstructure development. Figure 5(b) reveals the microstructure of the SZ, characterized by the presence of dynamically recrystallized grains, and thus dynamic recrystallization is evidenced. Dynamic recrystallization occurs when the welding is subject to both severe plastic deformation and high frictional heat. Furthermore, it is reported that the Al_2O_3 nanoparticles at SZ might have undergone stretching, and thus contributed significantly to grain refinement, as seen in Figure 5(b).[53] The TMAZ, undergoing plastic deformation under elevated temperatures, demonstrated enhanced grain refinement in contrast to the BM. Reduced grain size signifies and supports the dominant role of added nanoparticles within the weld region.

Metallurgical characterization of SZ

Figures 6 and 7 present the FESEM micrographs of the SZ prepared at 1000 rpm (the lowest rotational speed) and at 1400 rpm (optimal rotational speed). This provides insight of rotational speed and how it impacts the dispersion of nanoparticles at SZ. In the SZ of the weld sample produced at 1400 rpm (as shown in Figure 6), a uniform distribution of Al_2O_3 nanoparticles is observed, primarily along the grain boundaries, effectively impeded grain growth and consolidation. This uniform distribution contributes to the composite joint's higher lap shear fracture load (LSFL). Conversely, the sample prepared at a lower speed (1000 rpm) exhibits grouped nanoparticles both inside and outside the grains, with larger clusters (as shown in Figure 7).

The aggregation of Al_2O_3 nanoparticles results in an augmentation of the aluminum matrix and the interface area with Al_2O_3. This phenomenon indicates a bonding deficiency, attributed to reduced tool rotational speed leading to decreased heat generation. Consequently, microscopy images of the SZ reveal that insufficient heat and stirring action can have adverse effects on the even dispersion of Al_2O_3 nanoparticles and grain size reduction, as depicted in Figure 7.

Figure 8 presents the EDS and elemental mapping analysis results conducted in the SZ. The EDS pattern indicates prominent peaks for aluminum and oxygen, confirming the presence of Al_2O_3 nanoparticles in the weld area. The elemental mapping images demonstrate the homogeneous distribution and mixing of aluminum,

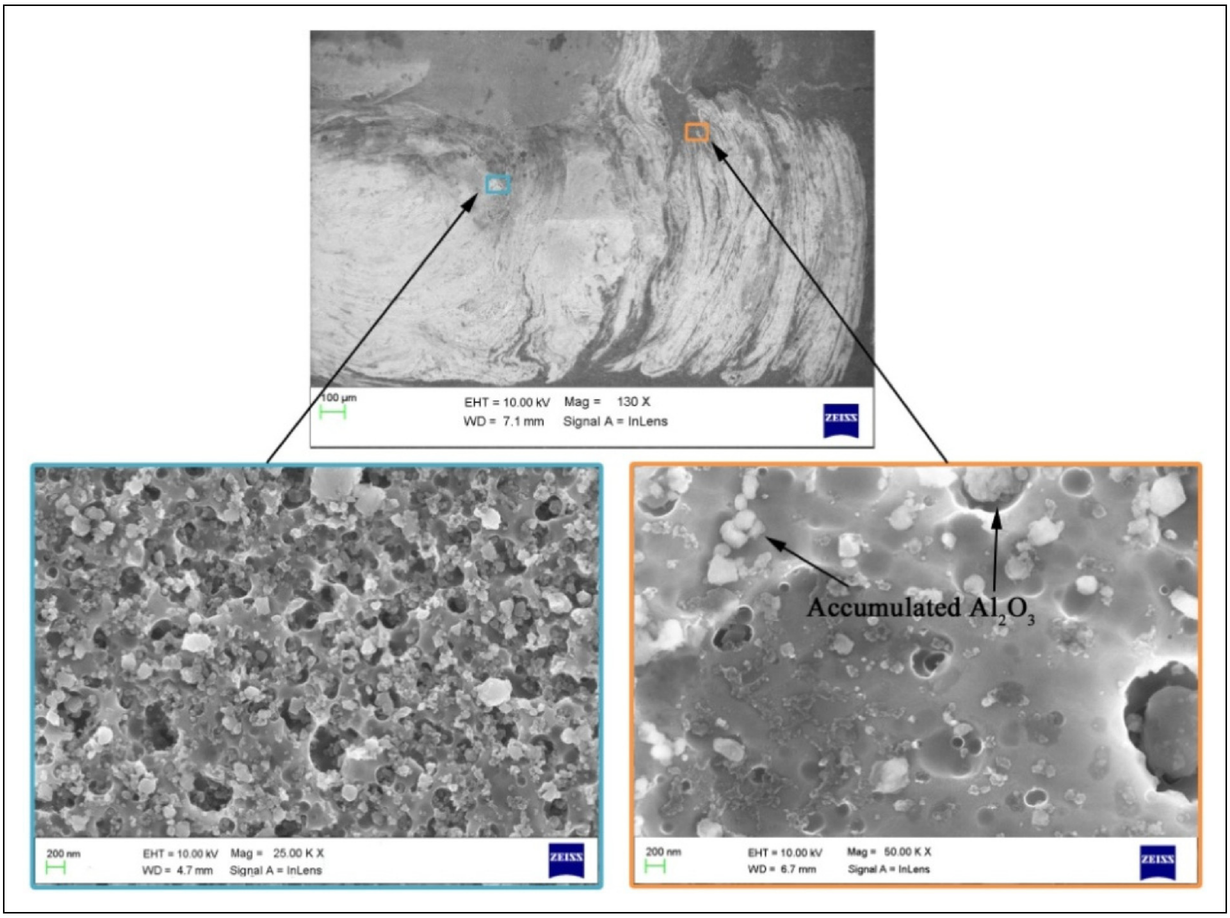

Figure 7. FESEM image of SZ at 1000 rpm tool speed.

oxygen, magnesium and copper elements, further confirming the incorporation of Al_2O_3 nanoparticles within the aluminum matrix. Importantly, no interfacial reaction from the images indicates a stable interface between the nanoparticles and the matrix.

Influence of tool rotation speed on LSFL

Figure 9 illustrates LSFL under different tool rotational speeds. The results illustrate a direct correlation between rotational speed and tensile strength, showing a steady rise until it reaches its maximum at 1400 rpm. However, beyond this point, the tensile strength starts to decline. The LSFL values for the joints at 1000, 1200, 1400 and 1600 rpm were recorded as 4790, 5250, 5780 and 5195 N, respectively. At the same rotational speed and room temperature, the LSFL of the joint reached 5780 N, showing a significant 18% increase compared to the LSFL of joints prepared without Al_2O_3 nanoparticles, which was measured as 4740 N. The error bars displayed in Figure 9(a) depict the standard deviation of LSFL across different tool rotational speeds, offering a measure of the consistency in joint strength.

It is significant to observe that welds produced at both lower and higher rotational speeds displayed a brittle fracture behavior. The fracture manifested within the nugget zone, as clearly depicted in Figure 9(b). This observation suggests that the reduction in strength can be ascribed to insufficient or excessive heat generation during the stirring process, which in turn resulted in inadequate material flow. Two key factors contribute to the observed trends in LSFL. Firstly, higher rotational speeds lead to elevated heat input, resulting in an increase in grain size and the dissolution of reinforced Al_2O_3 particles in the welded zone of AA 6061-T6 and AA7075-T6 materials.[57] Secondly, higher heat input induces increased turbulence in the plasticized materials undergoing strain, which facilitates the development of defects in the weld joints. The distribution of nanoparticles across different regions further affects the tensile properties observed at various rotation speeds.[58]

Fracture analysis reveals that fractures predominantly occur along the nugget region with increased rotational speed. In high-strength joints, fractures form at the interface of the nugget and BM, as evidenced in Figure 9(b). This indicates that the choice of rotational speed significantly impacts the distribution of Al_2O_3 nanoparticles and subsequently affects the fracture behavior and tensile strength of the joints.[59,60]

Fractography images from field emission scanning electron microscopy (FESEM) in Figure 10 reveal microvoid coalescence characteristics. Figure 10(a) shows the fracture surface of the sample at 1000 rpm, yielding the

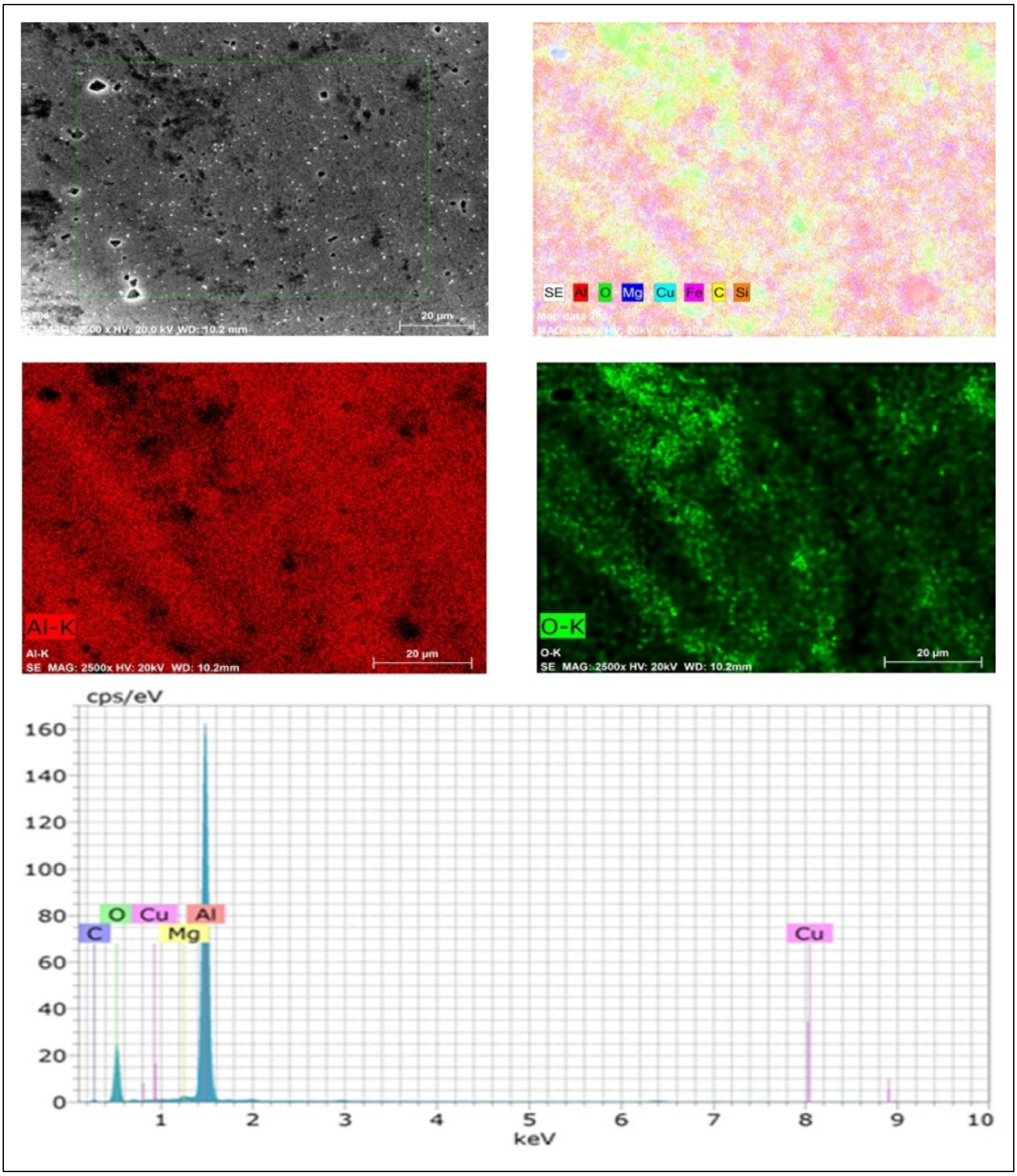

Figure 8. Elemental mapping and EDX result of the SZ of the sample fabricated at 1400 rpm.

minimum lap shear load, while Figure 10(b) depicts the sample at 1400 rpm with the maximum LSFL. Both surfaces exhibit dimples, indicating a ductile fracture.[61] The 1400 rpm weld displays finer dimples and more pronounced shear lips, suggesting greater plastic deformation. Interfacial failure between added nanoparticles and the aluminum matrix results in a larger number of smaller micro-voids in the 1400 rpm sample. Micro-void nucleation and coalescence characterize the fracture mechanisms in both surfaces. The 1400 rpm weld shows enhanced ductility, plastic deformation and increased micro-void formation, indicating superior strength compared to the 1000 rpm sample.

Conclusion

The influence of alumina nano-fillers and varying tool rotation speeds on the microstructural characteristics and mechanical characteristics of dissimilar aluminum FSW lap joints was investigated and reported below.

1. Investigating the highest rotation speed (1600 rpm) and lowest rotation speed (1000 rpm), it is understood that the higher the speed, the higher the homogeneous distribution and higher LSFL. The lowest speed results in the aggregated nanoparticles in the nugget zone, leading to inadequate bonding and reduced lap shear strength.

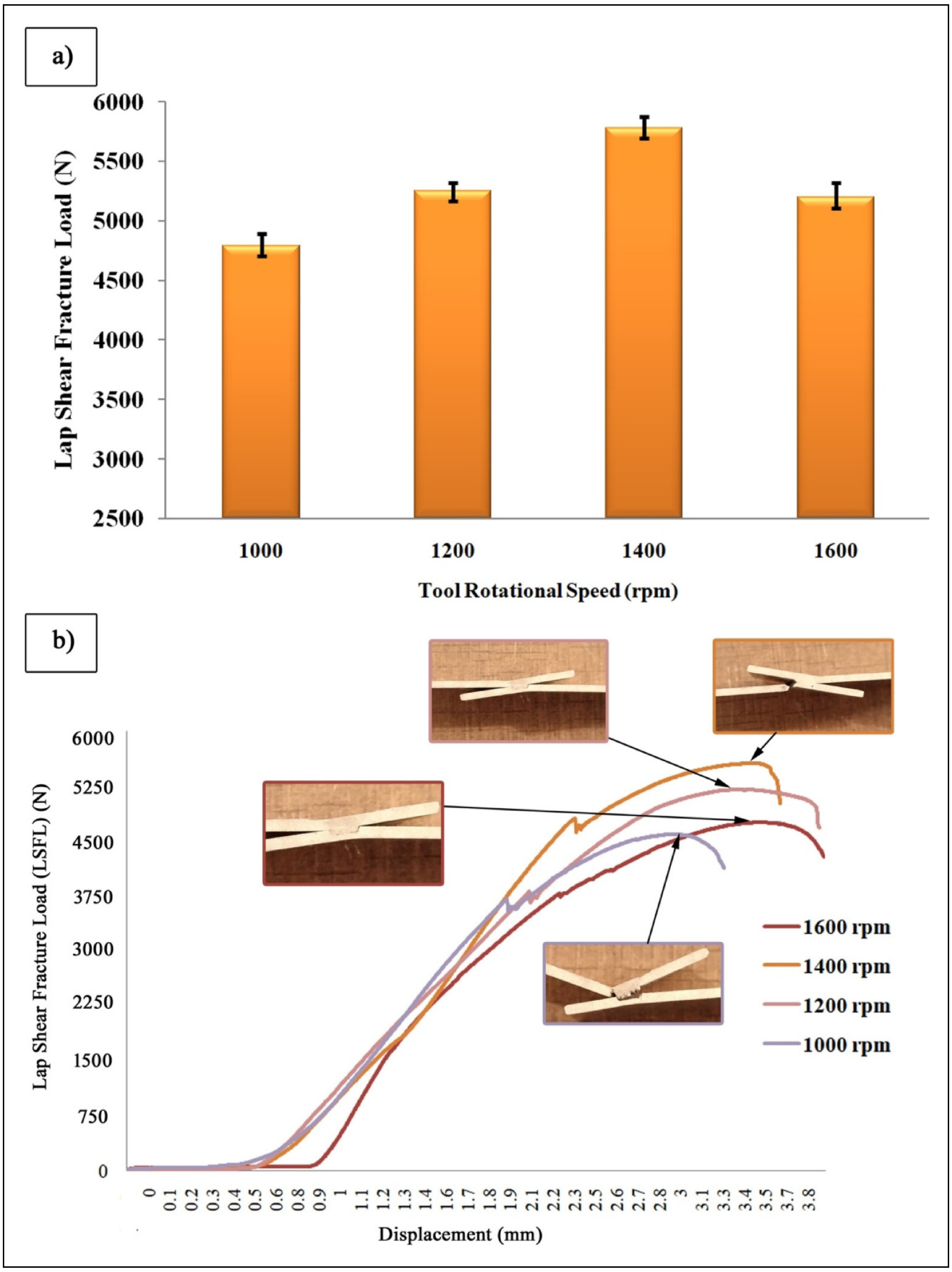

Figure 9. (a) LSFL at varying tool rotational speeds and (b) load-displacement graph with fractured samples.

2. The optimal rotation speed is found to be 1400 rpm, where nanoparticles were found along the grain boundaries, slightly enhanced grain refinement and consolidation. This is the best speed at which the highest lap shear strength was recorded. The decrease in strength at 1600 rpm was attributed to the poor dissolution of reinforced Al_2O_3 particles, increased turbulence and defect formation in the weld joints.
3. Inadequate production of heat and insufficient stirring action negatively affect the nanoparticle distribution and grain size uniformity within the SZ. The width of the SZ is observed to vary with the tool rotation speed. The reduced width was observed at the highest rotation speed.

The optimization of FSW parameters based on rotation speed and nanoparticle distribution can inform practical applications, leading to improved performance and reliability in joined aluminum components. The findings from this investigation could provide valuable insights related to friction stir-welded dissimilar lap joints, which can apprise the development of advanced joining techniques in the automotive and manufacturing industries.

Declaration of conflicting interests

The authors declared no potential conflicts of interest with respect to the research, authorship, and/or publication of this article.

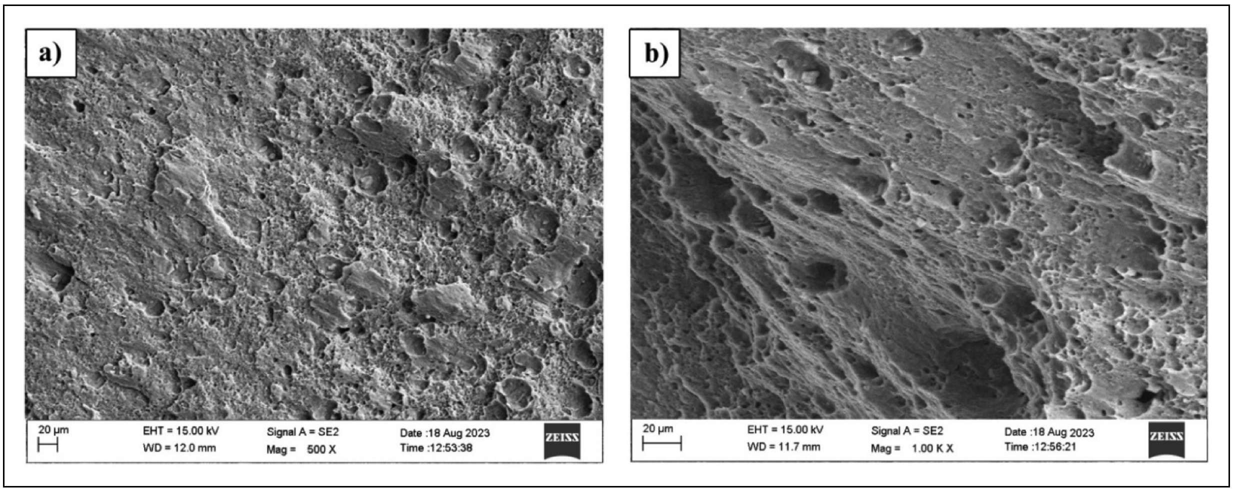

Figure 10. FESEM fractography of fracture surface of lap shear tested specimens prepared at (a) 1000 rpm and (b) 1400 rpm.

Funding

The authors received no financial support for the research, authorship, and/or publication of this article.

Supplemental material

Supplemental material for this article is available online.

ORCID iDs

S Suresh https://orcid.org/0000-0001-8840-0786
Elango Natarajan https://orcid.org/0000-0003-1215-0789

References

1. Jiang XJ, Bao SJ, Zhang LW, et al. Effect of Zr on microstructure and properties of TC4 alloy fabricated by laser additive manufacturing. *J Mater Res Technol* 2023; 24: 8782–8792.
2. Li M, Guo Q, Chen L, et al. Microstructure and properties of graphene nanoplatelets reinforced AZ91D matrix composites prepared by electromagnetic stirring casting. *J Mater Res Technol* 2022; 21: 4138–4150.
3. Satheesh C, Pandian S and Senthil Kumar R. Experimental identification of optimized process parameters for FSW of AZ91C Mg alloy using quadratic regression models. *Strojniški Vestn – J Mech Eng* 2020; 66: 736–751.
4. Fu ZH, Yang BJ, Shan ML, et al. Hydrogen embrittlement behavior of SUS301L-MT stainless steel laser-arc hybrid welded joint localized zones. *Corros Sci* 2020; 164: 108337.
5. Danish M, Ginta T, Yasir M, et al. Light alloys and their machinability: a review. In: Carou D and Davim JP (eds) *Machining of light alloys aluminum, titanium, and magnesium*. CRC Press Taylor & Francis Group, 2018, pp.1–34.
6. Tisza M and Czinege I. Comparative study of the application of steels and aluminium in lightweight production of automotive parts. *Int J Light Mater Manuf* 2018; 1: 229–238.
7. Suresh S, Venkatesan K and Natarajan E. Influence of SiC nanoparticle reinforcement on FSS welded 6061-T6 aluminum alloy. *J Nanomater* 2018; 2018: 1–11.
8. Dimopoulos A, Vairis A, Vidakis N, et al. On the friction stir welding of Al 7075 thin sheets. *Metals (Basel)* 2020; 11: 57.
9. Kang M and Kim C. A review of joining processes for high strength 7xxx series aluminum alloys. *J Weld Join* 2017; 35: 79–88. Epub ahead of print 2017.
10. Akbari M, Asadi P and Sadowski T. A review on friction stir welding/processing: numerical modeling. *Materials (Basel)* 2023; 16: 5890.
11. Chen Y, Sun S, Zhang T, et al. Effects of post-weld heat treatment on the microstructure and mechanical properties of laser-welded NiTi/304SS joint with Ni filler. *Mater Sci Eng A* 2020; 771: 138545.
12. Tao W, Shuwei D, Matsuda K, et al. Dynamic recrystallization and dynamic precipitation in AA6061 aluminum alloy during friction stir welding. *Trans Indian Inst Met* 2022; 75: 1329–1339. Epub ahead of print 2022.
13. Ahmed S and Saha P. Development and testing of fixtures for friction stir welding of thin aluminium sheets. *J Mater Process Technol* 2018; 252: 242–248.
14. Khalafe WH, Sheng EL, Bin Isa MR, et al. The effect of friction stir welding parameters on the weldability of aluminum alloys with similar and dissimilar metals: review. *Metals (Basel)* 2022; 12: 2099.
15. Gain S, Sanyal D, Acharyya SK, et al. Friction stir welding of AISI-316L steel pipes: mechanical and metallurgical characterization of the joint. *Proc Inst Mech Eng Part E J Process Mech Eng* 2022; 236: 2382–2393.
16. Feng Y, Pan R, Zhou T, et al. Direct joining of quartz glass and copper by nanosecond laser. *Ceram Int* 2023; 49: 36056–36070.
17. Zhu ZY, Liu YL, Gou GQ, et al. Effect of heat input on interfacial characterization of the butter joint of hot-rolling CP-Ti/Q235 bimetallic sheets by Laser + CMT. *Sci Rep* 2021; 11: 10020.
18. Akbari M, Asadi P, Aliha MRM, et al. Modeling and optimization of process parameters of the piston alloy-based composite produced by fsp using response surface methodology. *Surf Rev Lett* 2023; 30. DOI: 10.1142/s0218625×23500415.
19. Suresh S, Natarajan E, Vinayagamurthi P, et al. Optimum tool traverse speed resulting equiaxed recrystallized grains and high mechanical strength at swept friction stir spot welded AA7075-T6 lap joints. In: Natarajan E, Vinodh S and Rajkumar V (eds) *Materials, design and manufacturing for sustainable environment*. Singapore: Springer Nature Singapore, 2023, pp.547–555.

20. Chen F, Zhang H, Li Z, et al. Residual stresses effects on fatigue crack growth behavior of rib-to-deck double-sided welded joints in orthotropic steel decks. *Adv Struct Eng* 2024; 27: 35–50. Epub ahead of print 8 November 2023.
21. Astarita A, Tucci F, Silvestri AT, et al. Dissimilar friction stir lap welding of AA2198 and AA7075 sheets: forces, microstructure and mechanical properties. *Int J Adv Manuf Technol* 2021; 117: 1045–1059.
22. Grong Ø, Sandnes L and Berto F. Progress in solid state joining of metals and alloys. *Procedia Struct Integr* 2019; 17: 788–798.
23. Gerlich AP. Welding and joining of light alloys. In: Caballero FG (ed) *Encyclopedia of materials: metals and alloys. Elsevier*, 2022: pp.234–244. DOI: 10.1016/B978-0-12-819726-4.00063-6.
24. Gite RA, Loharkar PK and Shimpi R. Friction stir welding parameters and application: a review. *Mater Today Proc* 2019; 19: 361–365.
25. Akbari M, Asiabaraki HR and Aliha M. Investigation of the effect of welding and rotational speed on strain and temperature during friction stir welding of AA5083 and AA7075 using the CEL approach. *Eng Res Express* 2023; 5: 025012.
26. P S IJS and, et al. JG. Establishment of empirical relations amidst mechanical attributes of friction stir welded distinctive alloys of Mg and optimized process parameters. *Mater Res Express* 2023; 10: 066502.
27. Singh VP, Patel SK, Ranjan A, et al. Recent research progress in solid state friction-stir welding of aluminium–magnesium alloys: a critical review. *J Mater Res Technol* 2020; 9: 6217–6256.
28. Suresh S, Venkatesan K, Natarajan E, et al. Evaluating weld properties of conventional and swept friction stir spot welded 6061-T6 aluminium alloy. *Mater Express* 2019; 9: 851–860.
29. Anton Savio Lewise K and Edwin Raja Dhas J. FSSW process parameter optimization for AA2024 and AA7075 alloy. *Mater Manuf Process* 2022; 37: 34–42.
30. Sudhagar S and Gopal PM. Investigation on mechanical and tribological characteristics Cu/Si3N4 surface composite developed through friction stir processing. *Silicon* 2022; 14: 4207–4216
31. Anand R and Padmanabhan R. An integrated ANN and design of experiments technique to optimize the FSW input parameters of novel interlock lap weld. *Proc Inst Mech Eng Part E: J. Process. Mech Eng* 2023; 238: 213–226.
32. Yaknesh S, Sampathkumar K and Sevvel P. Effect of tool pin geometry and process parameters during FSW of dissimilar alloys of Mg. *Mater Res* 2022; 25: e20210508.
33. Sevvel P, Satheesh C and Jaiganesh V. Influence of tool rotational speed on microstructural characteristics of dissimilar Mg alloys during friction stir welding. *Trans Can Soc Mech Eng* 2019; 43: 132–141.
34. Huang Y, Meng X, Zhang Y, et al. Micro friction stir welding of ultra-thin Al-6061 sheets. *J Mater Process Technol* 2017; 250: 313–319.
35. Liu FJ, Fu L and Chen HY. Microstructure evolution and fracture behaviour of friction stir welded 6061-T6 thin plate joints under high rotational speed. *Sci Technol Weld Join* 2018; 23: 333–343.
36. Rajesh S and Badheka VJ. Effect of friction stir lap weld and post weld heat treatment on corrosion behavior of dissimilar aluminum alloys. *Proc Inst Mech Eng Part L J Mater Des Appl* 2019; 233: 1053–1064.
37. Song Y, Yang X, Cui L, et al. Defect features and mechanical properties of friction stir lap welded dissimilar AA2024–AA7075 aluminum alloy sheets. *Mater Des* 2014; 55: 9–18.
38. Qiao K, Zhang T, Wang K, et al. Effect of multi-pass friction stir processing on the microstructure evolution and corrosion behavior of ZrO2/AZ31 magnesium matrix composite. *J Mater Res Technol* 2022; 18: 1166–1179.
39. Singh T, Tiwari SK and Shukla DK. Effects of Al 2 O 3 nanoparticles volume fractions on microstructural and mechanical characteristics of friction stir welded nanocomposites. *Nanocomposites* 2020; 6: 76–84.
40. Suresh S, Venkatesan K and Rajesh S. Optimization of process parameters for friction stir spot welding of AA6061/Al2O3 by Taguchi method. In: AIP Conference Proceedings, pp.030018.
41. Suresh S, Elango N, Venkatesan K, et al. Sustainable friction stir spot welding of 6061-T6 aluminium alloy using improved non-dominated sorting teaching learning algorithm. *J Mater Res Technol* 2020; 9: 11650–11674.
42. AbuShanab WS and Moustafa EB. Effects of friction stir processing parameters on the wear resistance and mechanical properties of fabricated metal matrix nanocomposites (MMNCs) surface. *J Mater Res Technol* 2020; 9: 7460–7471.
43. Bharti S, Ghetiya ND and Patel KM. A review on manufacturing the surface composites by friction stir processing. *Mater Manuf Process* 2021; 36: 135–170.
44. Suresh S, Venkatesan K, Natarajan E, et al. Performance analysis of nano silicon carbide reinforced swept friction stir spot weld joint in AA6061-T6 alloy. *Silicon* 2021; 13: 3399–3412.
45. Babu S, Elangovan K, Balasubramanian V, et al. Optimizing friction stir welding parameters to maximize tensile strength of AA2219 aluminum alloy joints. *Met Mater Int* 2009; 15: 321–330.
46. West M, Jasthi B, Hosemann P, et al. Friction stir welding of oxide dispersion strengthened alloy MA956 In: Mishra RS, Mahoney MW, Sato Y, et al. (eds) *Friction stir welding and processing VI*. Hoboken, NJ: John Wiley & Sons, 2011. DOI: 10.1002/9781118062302.ch5.
47. Abbass MK and Raheef KM. Evaluation of the mechanical properties of friction stir lap welded joints for dissimilar aluminum alloys(AA1100 to AA6061). In: 2018 1st International Scientific Conference of Engineering Sciences - 3rd Scientific Conference of Engineering Science (ISCES), pp.192–197: IEEE.
48. Masoumi Khalilabad M, Zedan Y, Texier D, et al. Effect of tool geometry and welding speed on mechanical properties of dissimilar AA2198–AA2024 FSWed joint. *J Manuf Process* 2018; 34: 86–95.
49. Vimalraj C and Kah P. Experimental review on friction stir welding of aluminium alloys with nanoparticles. *Metals (Basel)* 2021; 11: 390.
50. Jain S and Mishra RS. Effect of Al2O3 nanoparticles on microstructure and mechanical properties of friction stir-welded dissimilar aluminum alloys AA7075-T6 and AA6061-T6. *Proc Inst Mech Eng Part E J Process Mech Eng* 2022; 236: 1511–1521.
51. Jasiūnienė E, Žukauskas E, Dragatogiannis DA, et al. Investigation of dissimilar metal joints with nanoparticle fillers. *NDT E Int* 2017; 92: 122–129.
52. Kumar M, Das A and Ballav R. Influence of the Zn interlayer on the mechanical strength, corrosion and

microstructural behavior of friction stir-welded 6061-T6 aluminium alloy and AZ61 magnesium alloy dissimilar joints. *Mater Today Commun* 2023; 35: 105509.

53. Mohamed S, Yoshiaki M, Kohsaku U, et al. Microstructural evolution of aluminium in dissimilar A1050/S45C FSW joints by Zn interlayer. *Mater Sci Technol* 2023; 39: 2722–2729.
54. Rabiezadeh A, Arghavani F and Mokhtari M. Effect of adding CNT on dissimilar welding of aluminium alloys by FSW. *Trans Indian Inst Met* 2021; 74: 1883–1894. Epub ahead of print 2021.
55. Paranthaman V, Sundaram KS and Natrayan L. Influence of SiC particles on mechanical and microstructural properties of modified interlock friction stir weld lap joint for automotive grade aluminium alloy. *Silicon* 2022; 14: 1617–1627.
56. Natrayan L, Ravichandran M, Veeman D, et al. Enhancement of mechanical properties on novel friction stir welded Al-Mg-Zn alloy joints reinforced with nano-SiC particles. *J Nanomater* 2021; 2021: 1–10.
57. Suresh S, Natarajan E, Shanmugam R, et al. Strategized friction stir welded AA6061-T6/SiC composite lap joint suitable for sheet metal applications. *J Mater Res Technol* 2022; 21: 30–39.
58. Suresh S, Natarajan E, Franz G, et al. Differentiation in the SiC filler size effect in the mechanical and tribological properties of friction-spot-welded AA5083-H116 alloy. *Fibers* 2022; 10: 109.
59. Suresh S, Natarajan E, Franz G, et al. Influences of nanoparticles in friction stir welding processes. In: Boopathi S and Davim JP (eds) *Sustainable utilization of nanoparticles and nanofluids in engineering applications*. Hershey, PA: IGI Global, 2023, pp.32-55. DOI: 10.4018/978-1-6684-9135-5.ch002
60. Yuhua C, Yuqing M, Weiwei L, et al. Investigation of welding crack in micro laser welded NiTiNb shape memory alloy and Ti6Al4 V alloy dissimilar metals joints. *Opt Laser Technol* 2017; 91: 197–202.
61. Suresh S, Venkatesan K, Natarajan E, et al. Influence of tool rotational speed on the properties of friction stir spot welded AA7075-T6/Al2O3 composite joint. In: Materials Today: Proceedings, pp. 62–67.